CrystEngComm

ROYAL SOCIETY OF CHEMISTRY

PAPER

View Article Online
View Journal | View Issue

Cite this: *CrystEngComm*, 2025, **27**, 1736

Fine-tuning of gas uptake and selectivity in a hexafluorozirconate pillared coordination network that features two porous phases†

Nathan C. Harvey-Reid, [a] Hayley S. Scott,[a] Komal M. Patil, [a] Naveen Kumar,[c] Colm Healy,[ab] Michael J. Zaworotko, [c] Soumya Mukherjee *[c] and Paul E. Kruger *[a]

Received 11th December 2024,
Accepted 6th February 2025

DOI: 10.1039/d4ce01250j

rsc.li/crystengcomm

Hybrid coordination networks, sustained by divalent transition metal ions and a combination of organic and inorganic linker ligands, are an emerging class of physisorbents for adsorptive gas and vapour capture, especially under trace (≤1%) concentrations. Herein, we report a Cu(II) hybrid coordination network using the anionic pillar hexafluorozirconate ZrF_6^{2-}, $[Cu(pypz)_2ZrF_6]_n$; ZRFSIX-21-Cu (21 = 4-(3,5-dimethyl-1*H*-pyrazol-4-yl)pyridine). ZRFSIX-21-Cu possesses two ultramicroporous phases, a two-dimensional square lattice phase (α), and a three-dimensional primitive cubic unit phase (β), a rarity among hybrid ultramicroporous materials. Interestingly, **ZRFSIX-21-Cu-α** revealed better selectivity for C_2H_2 over CO_2, and **ZRFSIX-21-Cu-β** for C_2H_2 over C_2H_4.

Introduction

Hybrid ultramicroporous materials (HUMs),[1] a subfamily of hybrid coordination networks (HCNs), have emerged as a class of porous physisorbents suitable for gas separations.[1–3] By taking advantage of ultramicroporous channels (<7 Å) and highly fluorinated pillars (SiF_6^{2-}, TiF_6^{2-}, *etc.*), HUMs offer strong electrostatic-rich high density of sorbate binding sites. Such strong binding often enables HUMs to demonstrate i) highly selective trace gas capture; ii) record-high binary and multicomponent gas separations (CO_2/N_2, C_2H_2/CO_2, C_2H_2/C_2H_4; $C_2H_2/C_2H_4/CO_2$, $C_2H_2/C_2H_4/CH_4$, among others).[2,4] Owing to their modular nature and amenability to the crystal engineering design principles, new HUMs can be readily synthesized.[5] Simply put, fine-tuning of components within the core blueprint of HUMs enables superior control of their pore environment. This is key to optimising the resulting performance parameters,[2] such as gas uptake, binding energy, selectivity, and separation potential.[6–8] To optimise these aspects, several iterations of HUMs have been synthesized, often by varying the inorganic pillaring linkers. These include the first and second generation HUMs, namely, **MFSIX** (SiF_6^{2-}, TiF_6^{2-}, GeF_6^{2-}),[8,9] **DICRO** ($Cr_2O_7^{2-}$),[10] **MOFFIVE** ($NbOF_5^{2-}$, $TaOF_5^{2-}$),[11] **MFFIVE** (AlF_5^{2-}, FeF_5^{2-}),[12] and the **mmo** nets (CrO_4^{2-}, MoO_4^{2-}, WO_4^{2-}).[13]

Traditionally, the above-mentioned HUMs relied upon pyrazine or pyridyl linkers to dictate pore size and/or promote interpenetration.[7] The latest generation of HUMs have advanced this area by utilizing other *N*-heterocyclic derivatives, namely pyrazole. A recent report demonstrated the crystal engineering of a series of HUMs incorporating 4-(3,5-dimethyl-1*H*-pyrazol-4-yl) pyridine (**pypz**).[14] Inclusion of this ligand into the HUM platform afforded materials possessing both high selectivity and working capacity of C_2H_2 over CO_2.[15] Additionally, use of such ligands has been found to promote increased hydrolytic stability, which has been a prevalent issue in both HUMs and metal–organic materials (MOMs), in general.[16,17] Previous studies have shown that exposure to water or water vapour in HUMs typically leads to a structural transformation of the 3D **pcu** network to a 2D square lattice **sql** or **sql-c*** network. In the latter case, the square grids are interlocked, and the pillaring anions displaced, resulting in non-porous structures (Fig. 1).[17,18]

To further explore the capabilities of the **pypz** ligand within a HUM platform, we report here the synthesis of $[Cu(pypz)_2ZrF_6]_n$ (**ZRFSIX-21-Cu**), a new HUM featuring the ZrF_6^{2-} pillar. Unlike its parent HUM, **SIFSIX-21-Cu**,[15] **ZRFSIX-**

[a] *MacDiarmid Institute for Advanced Materials and Nanotechnology, School of Physical and Chemical Sciences, University of Canterbury, Private Bag 4800, Christchurch 8140, New Zealand. E-mail: paul.kruger@canterbury.ac.nz*
[b] *Department of Chemistry, Harvey Mudd College, 301 Platt Blvd, Claremont, CA 91711, USA*
[c] *Department of Chemical Sciences, Bernal Institute and Research Ireland Centre for Pharmaceuticals (SSPC), University of Limerick, Limerick V94 T9PX, Ireland. E-mail: Soumya.Mukherjee@ul.ie*

† Electronic supplementary information (ESI) available: Experimental details, syntheses and characterisations: infrared spectra, thermogravimetric traces, powder X-ray diffractograms, gas sorption isotherms, *etc.* CCDC deposition entries 2408456 and 2408457. For ESI and crystallographic data in CIF or other electronic format see DOI: https://doi.org/10.1039/d4ce01250j

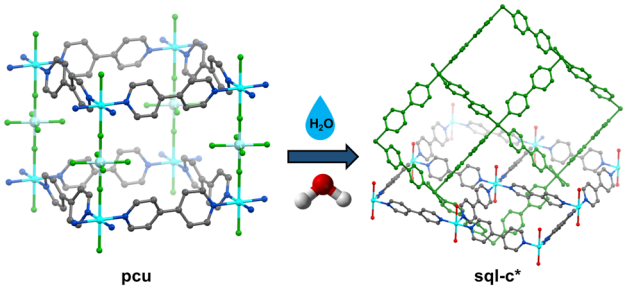

Fig. 1 Illustration showing the phase transition of a prototypical **pcu** topology HUM to an **sql-c*** topology CN, in the presence of excess water.

21-Cu exists in two distinct ultramicroporous phases, a 2D square lattice (**sql**) α-phase and a conventional 3D pillared **pcu** β-phase. Strikingly, and different to other anion-pillared HUMs, **ZRFSIX-21-Cu** is shown also to be porous in its 2D phase, a first in this family of materials. The work here reveals the structural differences between the phases and the impact these have on the porosity and separation potential for different gas mixtures.

Results and discussion

Synthesis and structural characterization

Single crystals of **ZRFSIX-21-Cu-α** were isolated following the evaporation of an acetonitrile solution containing a mixture of pypz, Cu^{2+} and ZrF_6^{2-}, whereas single crystals of **ZRFSIX-21-Cu-β** were obtained through layering the reagents atop each other in methanol at room temperature. Bulk samples of the α-phase were synthesized directly by mixing the reagents in acetonitrile, whereas methanol solvent afforded the β-phase (see synthesis section of ESI† for further details). Single-crystal X-ray diffraction (SC-XRD) revealed that **ZRFSIX-21-Cu-β** is isostructural to the previously reported pypz-based HUMs (**SIFSIX-21-Cu**, **SIFSIX-21-Ni**, *etc.*), crystallising as a **pcu** topology framework in the orthorhombic space group *Pnna*.[15] Whereas **ZRFSIX-21-Cu-α** crystallises as an **sql** network in the orthorhombic space group $Pna2_1$, it can be characterised as an incomplete or intermediate phase in the formation of **ZRFSIX-21-Cu-β**. The key difference between the two phases is that **ZRFSIX-21-Cu-α** contains only one axially bound ZrF_6^{2-} anion per Cu^{2+} node, rather than two, resulting in a square pyramidal $\{N_4F\}$ coordination chromophore around the Cu(II) centre (Fig. S1†). The absence of a second axial ZrF_6^{2-} anion in **ZRFSIX-21-Cu-α** leads to sequential **sql** layers exhibiting AB stacking, instead of being locked into a **pcu** network (Fig. S2†).

Ultramicroporosity is present in both phases due to one-dimensional channels aligned along the crystallographic *c*-axis for α and *b*-axis for β, respectively. **ZRFSIX-21-Cu-α** was found to feature a minimum pore window of *ca.* 2.5 Å, and a maximum pore window of *ca.* 6.0 Å (Fig. 2a and b). In **ZRFSIX-21-Cu-β**, the pore window was determined at *ca.* 4.8 Å, comparable to the isostructural HUM, **SIFSIX-21-Cu** (4.5 Å), and **TIFSIX-4-Cu** (4.7 Å) (Fig. 2c).[15] Interestingly, the pore chemistry of **ZRFSIX-21-Cu-α** resembles that of the previously reported **sql** HUM, **sql-16-Cu-NO_3-α** (**16** = 4,4′-(2,5-dimethyl-1,4-phenylene)dipyridine).[19] In both cases, the pore window is partially occupied by the coordinating anion, causing the axial anions to interdigitate between the undulating 2D layers. The presence of the NO_3^- anion in **sql-16-Cu-NO_3-α** contributed to strong sorbent–sorbate interactions observed for C_2H_2 compared with CO_2,[19] suggesting a similar effect might be observed with the ZrF_6^{2-} anion in **ZRFSIX-21-Cu-α**.

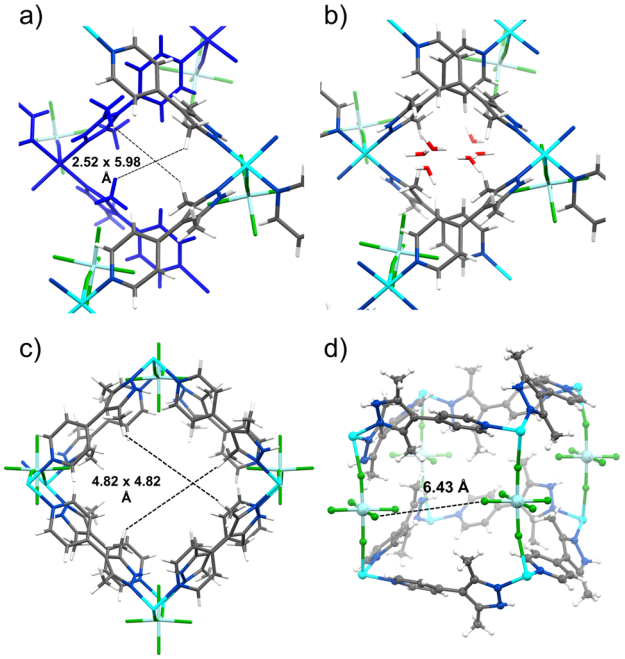

Fig. 2 Crystal structures of **ZRFSIX-21-Cu** (α and β). (a) Ultramicropores of **ZRFSIX-21-Cu-α** generated through AB stacking of 2D layers. (b) Packing of the guest solvent molecules within the pores of **ZRFSIX-21-Cu-α**. (c) Ultramicropores of 3D **ZRFSIX-21-Cu-β**. (d) ZrF_6^{2-} pillars of **ZRFSIX-21-Cu-β** used to generate the 3D structure and to potentially facilitate strong sorbate binding sites (due to short F–F distances between the neighbouring pillars). Colour code: Cu (cyan), Zr (pale blue), F (green), N (blue), C (grey) and H (white).

Powder X-ray diffraction (PXRD) was employed to confirm the bulk phase purity of **ZRFSIX-21-Cu-α** and **β**, as well as to verify the structural distinction between the two materials (**sql** *vs.* **pcu**). The PXRD diffractogram recorded after air drying revealed that **ZRFSIX-21-Cu-α** exists in a desolvated α′ phase, as indicated by subtle differences between the simulated and experimental diffractograms. Thermogravimetric analysis (TGA) showed thermal decomposition occurring at 473 K and 538 K for **ZRFSIX-21-Cu-α** and **ZRFSIX-21-Cu-β**, respectively (Fig. S5†).

Phase transition studies

To establish the relationship between and interconversion of **ZRFSIX-21-Cu-α** and **ZRFSIX-21-Cu-β** phases, we conducted a

series of experiments to track the transition between crystals of the α and β phases.

When soaked in a solution of MeOH, violet crystals of **ZRFSIX-21-Cu-α** were observed to slowly undergo a gradual phase transition to yield characteristic light-blue crystals of the **ZRFSIX-21-Cu-β** phase, over a period of 48 hours (Fig. S42†). PXRD measurements showed that in 24 hours, the sample comprised of a mixture of α and β phases, with complete conversion to **ZRFSIX-21-Cu-β** observed at 48 hours (Fig. 3). TGA measurements also confirmed successful phase transition as the decomposition profile complements that of the directly synthesized **ZRFSIX-21-Cu-β** (Fig. S5†). Attempts to reverse the phase change through heating crystals of **ZRFSIX-21-Cu-β** in acetonitrile or water to regenerate **ZRFSIX-21-Cu-α** were unsuccessful, suggesting thermodynamic stability of the β phase over the α phase.

Attempts were also made to induce a phase transition through direct heating of dried **ZRFSIX-21-Cu-α** to remove any residual solvent and potentially enable the ZrF_6^{2-} anions to lock the 2D layers together, forming **ZRFSIX-21-Cu-β**. These efforts were inspired by our previous work on the HUM **SIFSIX-3-Ni**, where the 3D material was realised by heating the **sql** precursor at 80 °C under vacuum. Heating **ZRFSIX-21-Cu-α** at 120 °C under vacuum resulted in the formation of an additional poly-crystalline phase, **ZRFSIX-21-Cu-γ** (Fig. S6 and S8†), distinguishable by its green colour (Fig. 4). No phase transition was observed below 120 °C, with **ZRFSIX-21-Cu-α** remaining unchanged.

Gas adsorption studies

Single-component gas adsorption studies were conducted on all three phases to evaluate their porosity. Activation of **ZRFSIX-21-Cu-α** at 50 °C and 120 °C under vacuum generated the phases **ZRFSIX-21-Cu-α′** and **ZRFSIX-21-Cu-γ** (Fig. S6†), while **ZRFSIX-21-Cu-β** was activated at room temperature under vacuum. N_2 adsorption isotherms at 77 K revealed that

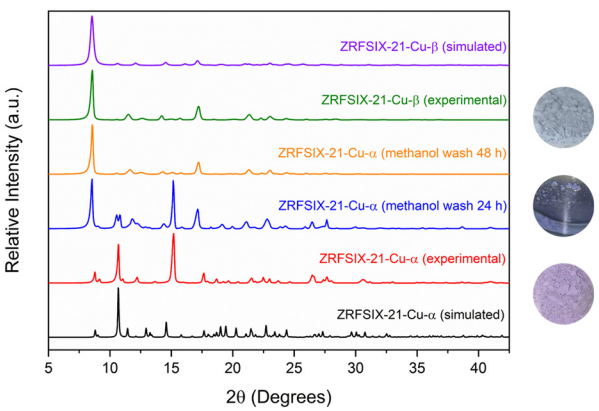

Fig. 3 PXRD patterns of **ZRFSIX-21-Cu**. **ZRFSIX-21-Cu-α** (red) undergoes a phase transition to **ZRFSIX-21-Cu-β** (green) upon treatment with methanol, over a 48 hour period (blue and yellow). Optical images on the right illustrate colour change observed during the α to β phase transition.

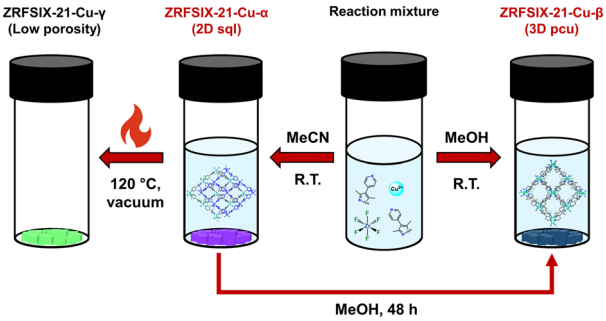

Fig. 4 Reaction pathways for the synthesis of **ZRFSIX-21-Cu-α**, **ZRFSIX-21-Cu-β** and **ZRFSIX-21-Cu-γ**.

both **ZRFSIX-21-Cu-α′** and **ZRFSIX-21-Cu-β** displayed typical type I isotherms, with BET surface areas calculated at 367 $m^2\ g^{-1}$ and 404 $m^2\ g^{-1}$, respectively, whereas **ZRFSIX-21-Cu-γ** showed no N_2 uptake (Fig. S9, S18 and S25†). Since **ZRFSIX-21-Cu-γ** was subjected to harsh activation at 120 °C under high vacuum, quality of the single crystals was no longer suitable for SC-XRD studies. Notably, the surface area of **ZRFSIX-21-Cu-β** was found to be markedly reduced compared to the other pypz-based HUMs, which typically report surface areas ranging from 747 $m^2\ g^{-1}$ to 931 $m^2\ g^{-1}$.[14] CO_2 isotherms at 195 K showed similar uptake levels and pore size distributions in **ZRFSIX-21-Cu-α′** and **ZRFSIX-21-Cu-β** (Fig. S9 and S18†), whereas **ZRFSIX-21-Cu-γ** exhibited lower CO_2 uptake at 195 K, resulting in a BET surface area of 343 $m^2\ g^{-1}$ (Fig. S25†). In **ZRFSIX-21-Cu-γ**, the lack of N_2 uptake and minimal CO_2 uptake at 195 K were further supported by no uptake observed across several other gas isotherms at 298 K (Fig. S26–S29†). The conspicuously low BET surface areas of **ZRFSIX-21-Cu-α′** and **ZRFSIX-21-Cu-β**, relative to other pypz-based HUMs, prompted us to explore their ability to adsorb CO_2 and C_2 gases under ambient conditions. C_2H_2, C_2H_4, and CO_2 adsorption isotherms were measured at 273, 283, and 298 K for **ZRFSIX-21-Cu-α′** and at 273 and 298 K for **ZRFSIX-21-Cu-β**. All measurements recorded at 273 K and above displayed type I isotherms.

ZRFSIX-21-Cu-α′ at ambient temperatures

At 1 bar and 298 K, the C_2H_2 uptake was 57.0 $cm^3\ g^{-1}$, while the CO_2 uptake was less than half this value, at 24.2 $cm^3\ g^{-1}$ (Fig. 5a).

The C_2H_2/CO_2 uptake ratio for **ZRFSIX-21-Cu-α′** was calculated to be 2.4, comparable to previously reported **sql** networks **UTSA-83a** (3.1)[20] and **sql-16-Cu-NO_3-α′** (2.1).[19] Although it has a lower uptake ratio, **ZRFSIX-21-Cu-α′** exhibits a much higher C_2H_2 uptake capacity, nearly five times that of **UTSA-83a** (57.0 $cm^3\ g^{-1}$ *vs.* 11.9 $cm^3\ g^{-1}$).[20] The isosteric enthalpies of adsorption (Q_{st}) for C_2H_2 and CO_2 were determined from the isotherms at 273, 283, and 298 K. Low-loading Q_{st} values for C_2H_2 (32.0 kJ mol^{-1}) and CO_2 (22.8 kJ mol^{-1}) were consistent with the significant difference in pure gas isotherm uptakes (Fig. 5c and S30†).

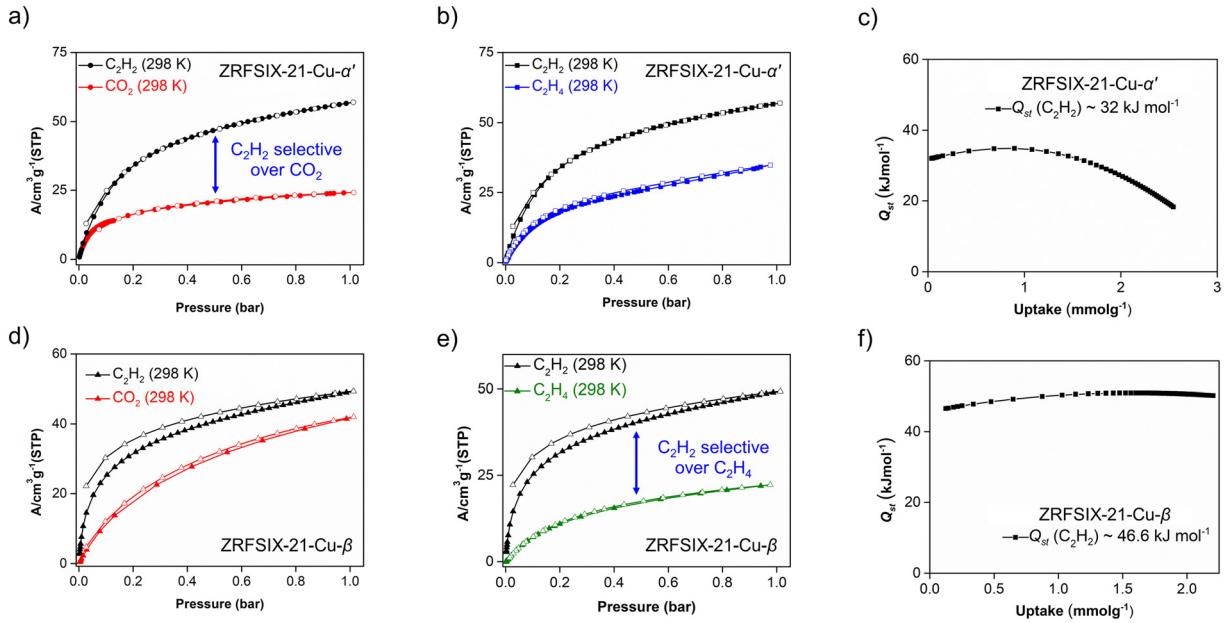

Fig. 5 Adsorption isotherms of **ZRFSIX-21-Cu-α′** for (a) C_2H_2 and CO_2 at 298 K and (b) C_2H_2 and C_2H_4 at 298 K. Closed and open symbols represent adsorption and desorption, respectively. (c) C_2H_2 adsorption enthalpy for **ZRFSIX-21-Cu-α′**. Adsorption isotherms of **ZRFSIX-21-Cu-β** for (d) C_2H_2 and CO_2 at 298 K and (e) C_2H_2 and C_2H_4 at 298 K respectively. (f) C_2H_2 adsorption enthalpy for **ZRFSIX-21-Cu-β**.

The selectivity of C_2H_2/CO_2 was determined using IAST by fitting the pure gas isotherms to the dual-site Langmuir–Freundlich equation. For a binary mixture of C_2H_2/CO_2 (1 : 1, v/v) at 1 bar and 298 K, the selectivity of C_2H_2/CO_2 was 4.8 (Fig. S34†), which is lower than that of **sql-16-Cu-NO$_3$-α′** (27.8)[19] and **UTSA-83a** (6.2),[20] yet still higher than several 3D C_2H_2 adsorbents such as **UTSA-220** (4.4),[21] **FJU-89a** (4.3),[22] **ZNU-8** (3.7),[23] **JNU-1** (3.0),[24] and **Zn-MOF-74** (2.0) (Fig. 6a).[25] Notably, at 1 bar and 283 K, the selectivity of **ZRFSIX-21-Cu-α′** increases significantly to 15.2, suggesting more favourable conditions for C_2H_2/CO_2 separation. With its relatively low binding energy and high C_2H_2 capacity, **ZRFSIX-21-Cu-α′** demonstrates potential as a versatile, C_2H_2-selective sorbent, with implications for mild regeneration conditions. Adsorption isotherms for C_2H_4 were also collected for **ZRFSIX-21-Cu-α′**, showing an uptake of 34.8 cm^3 g^{-1} at 1 bar and 298 K and a C_2H_2/C_2H_4 uptake ratio of 1.6 (Fig. 5b). However, similar Q_{st} values for C_2H_2 (32.0 kJ mol^{-1}) and C_2H_4 (30.7 kJ mol^{-1}) (Fig. 5c and S31†), along with a low selectivity of 1.7 (1 : 1, v/v), indicated that **ZRFSIX-21-Cu-α′** is not well-suited for C_2H_2/C_2H_4 separation (Fig. S34†).

ZRFSIX-21-Cu-β at ambient temperatures

As observed in isostructural analogues, **ZRFSIX-21-Cu-β** also demonstrated a higher affinity for C_2H_2 over CO_2, with uptakes of 49.4 cm^3 g^{-1} and 42.0 cm^3 g^{-1} at 1 bar and 298 K, respectively (Fig. 5d), and a significantly lower C_2H_4 uptake of 22.2 cm^3 g^{-1} (Fig. 5e). Although the C_2H_2/CO_2 uptake ratio for **ZRFSIX-21-Cu-β** is lower than that of **ZRFSIX-21-Cu-α′** (1.2 *vs.* 2.4), **ZRFSIX-21-Cu-β** exhibited superior uptake kinetics for C_2H_2 relative to CO_2. Calculated Q_{st} values revealed binding energies of 46.6 and 28.3 kJ mol^{-1} for C_2H_2 and CO_2 at zero loading, respectively (Fig. 5f and S32†). Compared to **ZRFSIX-21-Cu-α′**, **ZRFSIX-21-Cu-β** exhibits a much greater affinity for C_2H_2, with a difference of 14.6 kJ mol^{-1} in their C_2H_2 binding energies, while the CO_2 values remain relatively similar. This change in Q_{st} is likely due to differences in the pore environment between the α and β phases. Considering Q_{st} values at half-loading, an important metric for assessing 1 : 1 C_2H_2/CO_2 separations, the binding energy difference $(\Delta Q_{st})_{C_2H_2/CO_2}$ for **ZRFSIX-21-Cu-β** increases substantially to 28.5 kJ mol^{-1}. This $(\Delta Q_{st})_{C_2H_2/CO_2}$ value exceeds those of many high-performing C_2H_2/CO_2 selective materials, such as the **TCuX** series (X: Br, Cl, I; 5.5–8.2 kJ mol^{-1}),[26] **UTSA-74a** (6.0 kJ mol^{-1}),[27] **NKMOF-1-Ni** (9.5 kJ mol^{-1}),[28] and **sql-16-Cu-NO$_3$-α′** (11.4 kJ mol^{-1}).[19] Only benchmark materials such as **ATC-Cu** exhibit a greater $(\Delta Q_{st})_{C_2H_2/CO_2}$ at half-loading, a value heavily influenced by its exceptionally high binding energy for C_2H_2 (Q_{st} = 79.1 kJ mol^{-1}).[29]

As shown in previous studies of isostructural HUMs (*e.g.*, **SIFSIX-21-Ni**, **SIFSIX-21-Cu**),[15] **ZRFSIX-21-Cu-β** benefits from multiple ZrF_6^{2-} pillars and methyl groups that line the walls of the material. These features create strong electrostatic binding sites within the HUM, effectively trapping acetylene. **ZRFSIX-21-Cu-α′** can be considered an "incomplete" phase of **ZRFSIX-21-Cu-β**. SC-XRD analysis reveals that the ZrF_6 anions bound in **ZRFSIX-21-Cu-α′** are isolated from neighbouring ZrF_6^{2-} anions due to the interdigitation of **sql** layers, which could significantly reduce the effectiveness of the binding sites, limiting C_2H_2 interactions to a single ZrF_6^{2-} pillar and weaker interactions with the ligand. Furthermore, the larger ZrF_6^{2-} anion in **ZRFSIX-21-Cu-β** results in a greater

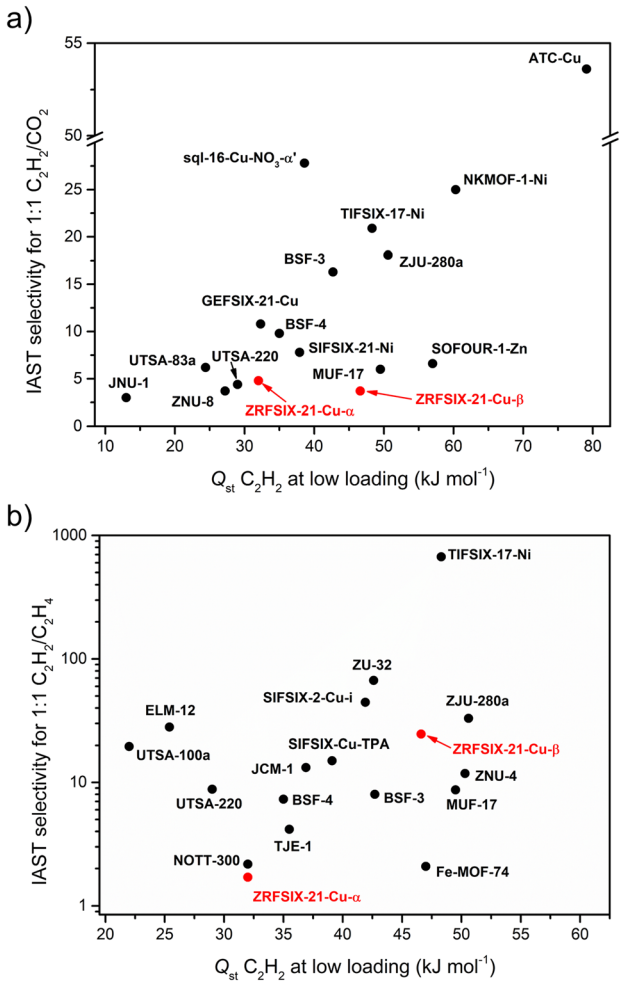

Fig. 6 Comparison scatter plot of C_2H_2 heat of adsorption and IAST selectivity for a) C_2H_2/CO_2 (1 : 1) and b) C_2H_2/C_2H_4 (1 : 1) of **ZRFSIX-21-Cu-α** and **ZRFSIX-21-Cu-β** with other top performing sorbents at 298 K. Molecular sieving materials have been omitted for clarity.

protrusion of F atoms into the pore windows due to longer Zr–F bonds (2.015 Å) and short F–F distances (6.43 Å) between adjacent ZrF_6^{2-} pillars (Fig. 2d), leading to a contracted pore volume and enhanced binding between sorbent and sorbate. IAST selectivity calculations for 1 : 1 binary mixture confirmed $S_{C_2H_2/CO_2}$ and $S_{C_2H_2/C_2H_4}$ values of 3.7 and 24.6 at 1 bar and 298 K, respectively (Fig. S35†), with C_2H_2/CO_2 selectivity comparable to **ZRFSIX-21-Cu-α′** ($S_{C_2H_2/CO_2}$ (1 : 1) = 4.8). With a selectivity of 24.6, **ZRFSIX-21-Cu-β** is well-suited for C_2H_2/C_2H_4 separation. However, these values still lag a few HUM physisorbents and other materials (Fig. 6b), such as the benchmark material **ZJU-300a**.[30] Additionally, **SIFSIX-14-Cu-i** and **UTSA-300a** exploit molecular sieving to achieve record-high selectivities.[31,32]

Conclusions

Ultramicroporous materials **ZRFSIX-21-Cu-α**, with a **sql** topology, and **ZRFSIX-21-Cu-β**, with a **pcu** topology, are additions to the MFSIX series of sorbents. Although they share an identical chemical formula, they form distinct structures due to variations in the Cu(II) coordination geometry and can be synthesised separately depending on the reaction conditions. Gas adsorption analysis revealed that both α and β phases are selective for C_2H_2, though unexpectedly, each favours a different gas pair. The α phase is more selective for C_2H_2 over CO_2, while the β phase shows higher selectivity for C_2H_2 over C_2H_4. Notably, IAST calculations indicate that **ZRFSIX-21-Cu-β** exhibits excellent C_2H_2/C_2H_4 selectivity (24.6). These newly discovered materials as physisorbents exemplify the nuances of crystal engineering and underscore the value of tuneable phases for specific gas separations.

Data availability

The data supporting this article have been included as part of the ESI.† Crystallographic data for **ZRFSIX-21-Cu-α** and **ZRFSIX-21-Cu-β** can be accessed from the Cambridge Crystallographic Data Centre (CCDC) as deposition numbers 2408456 and 2408457, respectively.

Author contributions

Conceptualization, N. C. H. R., S. M., M. J. Z., and P. E. K.; methodology, N. C. H. R., H. S. S. and K. M. P.; investigation, N. C. H. R., H. S. S., K. M. P., N. K. and S. M.; formal analysis, N. C. H. R., K. M. P., N. K., C. H., S. M. and P. E. K.; data curation, N. C. H. R., K. M. P., N. K., C. H., S. M. and P. E. K.; writing – original draft, N. C. H. R., S. M. and P. E. K.; writing – review & editing, all authors; funding acquisition, S. M., M. J. Z., and P. E. K.; supervision, S. M. and P. E. K.

Conflicts of interest

There are no conflicts to declare.

Acknowledgements

This publication arises from research supported by Research Ireland (formerly known as the Science Foundation Ireland) awarded to S. M., under grant number 21/PATH-S/9454. For open access, the authors have applied a CC BY public copyright licence to any author-accepted manuscript version of this submission. M. J. Z. and S. M. thank the SSPC Reward funding, AzAds. P. E. K. gratefully acknowledges the MacDiarmid Institute for Advanced Materials and Nanotechnology, and the School of Physical and Chemical Science at the University of Canterbury for financial and instrumental support.

Notes and references

1 S. Mukherjee and M. J. Zaworotko, *Trends Chem.*, 2020, **2**, 506–518.
2 (*a*) S. Mukherjee, D. Sensharma, K.-J. Chen and M. J. Zaworotko, *Chem. Commun.*, 2020, **56**, 10419–10441; (*b*) X.

Liu, H. Wang, C. Liu, J. Chen, Z. Zhou, S. Deng and J. Wang, *Chem Bio Eng.*, 2024, **1**(6), 469–487.

3 (*a*) Z. Ajoyan, P. Marino and A. J. Howarth, *CrystEngComm*, 2018, **20**, 5899–5912; (*b*) T. Wang, E. Lin, Y.-L. Peng, Y. Chen, P. Cheng and Z. Zhang, *Coord. Chem. Rev.*, 2020, **423**, 213485; (*c*) J. Dechnik, J. Gascon, C. J. Doonan, C. Janiak and C. J. Sumby, *Angew. Chem., Int. Ed.*, 2017, **56**, 9292–9310; (*d*) S. J. Datta, A. Mayoral, N. M. S. Bettahalli, P. M. Bhatt, M. Karunakaran, I. D. Carja, D. Fan, M. M. P. Graziane, R. Semino, G. Maurin, O. Terasaki and M. Eddaoudi, *Science*, 2022, **376**, 1080–1087.

4 (*a*) X. Li, H. Bian, W. Huang, B. Yan, X. Wang and B. Zhu, *Coord. Chem. Rev.*, 2022, **470**, 214714; (*b*) Y. Jiang, W. Yang, Y. Zhang, L. Wang and B. Chen, *J. Mater. Chem. A*, 2024, **12**, 5563–5580.

5 (*a*) S. Subramanian and M. J. Zaworotko, *Angew. Chem., Int. Ed. Engl.*, 1995, **34**, 2127–2129; (*b*) W. Lu, Z. Wei, Z.-Y. Gu, T.-F. Liu, J. Park, J. Park, J. Tian, M. Zhang, Q. Zhang, T. Gentle, M. Bosch and H.-C. Zhou, *Chem. Soc. Rev.*, 2014, **43**, 5561–5593.

6 (*a*) K. Uemura, A. Maeda, T. K. Maji, P. Kanoo and H. Kita, *Eur. J. Inorg. Chem.*, 2009, **16**, 2329–2333; (*b*) P. Nugent, Y. Belmabkhout, S. D. Burd, A. J. Cairns, R. Luebke, K. Forrest, T. Pham, S. Ma, B. Space, L. Wojtas, M. Eddaoudi and M. J. Zaworotko, *Nature*, 2013, **495**, 80; (*c*) S. K. Elsaidi, M. H. Mohamed, H. T. Schaef, A. Kumar, M. Lusi, T. Pham, K. A. Forrest, B. Space, W. Xu, G. J. Halder, J. Liu, M. J. Zaworotko and P. K. Thallapally, *Chem. Commun.*, 2015, **51**, 15530–15533.

7 A. Ebadi Amooghin, H. Sanaeepur, R. Luque, H. Garcia and B. Chen, *Chem. Soc. Rev.*, 2022, **51**, 7427–7508.

8 X. Cui, K. Chen, H. Xing, Q. Yang, R. Krishna, Z. Bao, H. Wu, W. Zhou, X. Dong, Y. Han, B. Li, Q. Ren, M. J. Zaworotko and B. Chen, *Science*, 2016, **353**, 141–144.

9 S.-i. Noro, S. Kitagawa, M. Kondo and K. Seki, *Angew. Chem., Int. Ed.*, 2000, **39**, 2081–2084.

10 (*a*) H. S. Scott, N. Ogiwara, K.-J. Chen, D. G. Madden, T. Pham, K. Forrest, B. Space, S. Horike, J. J. Perry IV, S. Kitagawa and M. J. Zaworotko, *Chem. Sci.*, 2016, **7**, 5470–5476; (*b*) H. S. Scott, S. Mukherjee, D. R. Turner, M. I. J. Polson, M. J. Zaworotko and P. E. Kruger, *CrystEngComm*, 2018, **20**, 1193–1197.

11 (*a*) A. Cadiau, K. Adil, P. M. Bhatt, Y. Belmabkhout and M. Eddaoudi, *Science*, 2016, **353**, 137–140; (*b*) B. Gao, Z. Zhang, J. Hu, L. Yang, Y. Li, L. Chen, X. Cui and H. Xing, *Chin. J. Chem. Eng.*, 2022, **42**, 49–54.

12 A. Cadiau, Y. Belmabkhout, K. Adil, P. M. Bhatt, R. S. Pillai, A. Shkurenko, C. Martineau-Corcos, G. Maurin and M. Eddaoudi, *Science*, 2017, **356**, 731–735.

13 M. H. Mohamed, S. K. Elsaidi, T. Pham, K. A. Forrest, H. T. Schaef, A. Hogan, L. Wojtas, W. Xu, B. Space, M. J. Zaworotko and P. K. Thallapally, *Angew. Chem., Int. Ed.*, 2016, **55**, 8285–8289.

14 N. Kumar, S. Mukherjee, N. C. Harvey-Reid, A. A. Bezrukov, K. Tan, V. Martins, M. Vandichel, T. Pham, L. M. van Wyk, K. Oyekan, A. Kumar, K. A. Forrest, K. M. Patil, L. J. Barbour, B. Space, Y. Huang, P. E. Kruger and M. J. Zaworotko, *Chem*, 2021, **7**, 3085–3098.

15 N. C. Harvey-Reid, D. Sensharma, S. Mukherjee, K. M. Patil, N. Kumar, S. J. Nikkhah, M. Vandichel, M. J. Zaworotko and P. E. Kruger, *ACS Appl. Mater. Interfaces*, 2024, **16**, 4803–4810.

16 A. J. Howarth, Y. Liu, P. Li, Z. Li, T. C. Wang, J. T. Hupp and O. K. Farha, *Nat. Rev. Mater.*, 2016, **1**, 15018.

17 D. O'Nolan, A. Kumar and M. J. Zaworotko, *J. Am. Chem. Soc.*, 2017, **139**, 8508–8513.

18 D. Sensharma, S. Vaesen, C. Healy, J. Hartmann, A. C. Kathalikkattil, P. Wix, F. Steuber, N. Zhu and W. Schmitt, *Eur. J. Inorg. Chem.*, 2018, **2018**, 1993–1997.

19 N. Kumar, S. Mukherjee, A. A. Bezrukov, M. Vandichel, M. Shivanna, D. Sensharma, A. Bajpai, V. Gascón, K. Otake and S. Kitagawa, *SmartMat*, 2020, **1**, e1008.

20 H. Cui, S. Chen, H. Arman, Y. Ye, A. Alsalme, R.-B. Lin and B. Chen, *Inorg. Chim. Acta*, 2019, **495**, 118938.

21 H. Li, L. Li, R.-B. Lin, G. Ramirez, W. Zhou, R. Krishna, Z. Zhang, S. Xiang and B. Chen, *ACS Sustainable Chem. Eng.*, 2019, **7**, 4897–4902.

22 Y. Ye, S. Chen, L. Chen, J. Huang, Z. Ma, Z. Li, Z. Yao, J. Zhang, Z. Zhang and S. Xiang, *ACS Appl. Mater. Interfaces*, 2018, **10**, 30912–30918.

23 Y. Zhang, W. Sun, B. Luan, J. Li, D. Luo, Y. Jiang, L. Wang and B. Chen, *Angew. Chem., Int. Ed.*, 2023, **62**, e202309925.

24 H. Zeng, M. Xie, Y. Huang, Y. Zhao, X. Xie, J. Bai, M. Wan, R. Krishna, W. Lu and D. Li, *Angew. Chem., Int. Ed.*, 2019, **58**, 8515–8519.

25 S. Xiang, W. Zhou, Z. Zhang, M. A. Green, Y. Liu and B. Chen, *Angew. Chem., Int. Ed.*, 2010, **49**, 4615–4618.

26 S. Mukherjee, Y. He, D. Franz, S. Wang, W. Xian, A. A. Bezrukov, B. Space, Z. Xu, J. He and M. J. Zaworotko, *Chem. – Eur. J.*, 2020, **26**, 4923–4929.

27 F. Luo, C. Yan, L. Dang, R. Krishna, W. Zhou, H. Wu, X. Dong, Y. Han, T.-L. Hu and M. O'Keeffe, *J. Am. Chem. Soc.*, 2016, **138**, 5678–5684.

28 Y.-L. Peng, T. Pham, P. Li, T. Wang, Y. Chen, K.-J. Chen, K. A. Forrest, B. Space, P. Cheng, M. J. Zaworotko and Z. Zhang, *Angew. Chem., Int. Ed.*, 2018, **57**, 10971–10975.

29 Z. Niu, X. Cui, T. Pham, G. Verma, P. C. Lan, C. Shan, H. Xing, K. A. Forrest, S. Suepaul, B. Space, A. Nafady, A. M. Al-Enizi and S. Ma, *Angew. Chem., Int. Ed.*, 2021, **60**, 5283–5288.

30 X. W. Gu, E. Wu, J. X. Wang, H. M. Wen, B. Chen, B. Li and G. Qian, *Sci. Adv.*, 2023, **9**, eadh0135.

31 B. Li, X. Cui, D. O'Nolan, H.-M. Wen, M. Jiang, R. Krishna, H. Wu, R.-B. Lin, Y.-S. Chen, D. Yuan, H. Xing, W. Zhou, Q. Ren, G. Qian, M. J. Zaworotko and B. Chen, *Adv. Mater.*, 2017, **29**, 1704210.

32 R.-B. Lin, L. Li, H. Wu, H. Arman, B. Li, R.-G. Lin, W. Zhou and B. Chen, *J. Am. Chem. Soc.*, 2017, **139**, 8022–8028.